Journal of Biomolecular NMR (2005) 31: 217–230
DOI 10.1007/s10858-005-0527-8

^{1}H–^{15}N correlation spectroscopy of nanocrystalline proteins

Corey R. Morcombe[a], Eric K. Paulson[a], Vadim Gaponenko[b], R. Andrew Byrd[b] & Kurt W. Zilm[a,*]
[a]*Department of Chemistry, Yale University, P.O. Box 208107, New Haven, CT 06520-8107, USA;* [b]*Structural Biophysics Laboratory, National Cancer Institute, Frederick, MD 21702, USA*

Received 23 March 2004; Accepted 20 December 2004

Key words: FSLG decoupling, high resolution solid state ^{1}H NMR, Lee–Goldburg decoupling, magnetic dilution, MAS ^{1}H NMR, solid state protein NMR

Abstract

The limits of resolution that can be obtained in ^{1}H–^{15}N 2D NMR spectroscopy of isotopically enriched nanocrystalline proteins are explored. Combinations of frequency switched Lee–Goldburg (FSLG) decoupling, fast magic angle sample spinning (MAS), and isotopic dilution via deuteration are investigated as methods for narrowing the amide ^{1}H resonances. Heteronuclear decoupling of ^{15}N from the ^{1}H resonances is also studied. Using human ubiquitin as a model system, the best resolution is most easily obtained with uniformly ^{2}H and ^{15}N enriched protein where the amides have been exchanged in normal water, MAS at ~20 kHz, and WALTZ-16 decoupling of the ^{15}N nuclei. The combination of these techniques results in average ^{1}H lines of only ~0.26 ppm full width at half maximum. Techniques for optimizing instrument stability and ^{15}N decoupling are described for achieving the best possible performance in these experiments.

Introduction

Although ^{1}H is the preferred nucleus in chemical applications of NMR spectroscopy to solution phase samples, dilute spin 1/2 nuclei such as ^{13}C and ^{15}N are more often used in NMR studies involving solid samples. This is simply a consequence of the fact that ^{1}H homonuclear dipolar couplings are difficult to suppress in solid state ^{1}H NMR spectra, and they dwarf the more chemically interesting ^{1}H chemical shifts. One approach has been to devise multiple pulse homonuclear decoupling schemes based on the NMR spectroscopist's ability to use radio frequency (RF) pulses to produce an average Hamiltonian consisting principally of chemical shift interactions (Waugh et al., 1968; Rhim et al., 1972). When combined with magnetization transfer to a dilute nucleus such as ^{13}C, and magic angle sample spinning (MAS) to average the anisotropy of the chemical shift, high quality solid state heteronuclear correlation (HETCOR) spectra can be obtained (Roberts et al., 1984). This type of spectroscopy is often the preferred means of obtaining ^{1}H chemical shifts in the solid state, being applicable to significantly larger systems than the combination of MAS and multiple pulse decoupling alone (CRAMPS) when single site resolution is required (Ryan et al., 1980). While the improvement in ^{1}H resolution using these sophisticated techniques is impressive, it nearly always falls short of what can be obtained for dilute nuclei such as ^{13}C and ^{15}N. In the majority of instances the superior resolution in the heteronuclear dimension of a solid state HETCOR is critical for resolving lines that

*To whom correspondence should be addressed. E-mail: kurt.zilm@yale.edu

overlap in the ^{1}H dimension, thereby making it possible to accurately determine the ^{1}H chemical shifts.

When MAS and multiple pulse decoupling are combined, one must be careful to make sure these two averaging techniques do not destructively interfere. The simplest approach to this problem is to make the cycle time for the multiple pulse dipolar decoupling much shorter than the MAS rotor period (Bronnimann et al., 1988; Olejniczak et al., 1984). At present, the frequency switched Lee–Goldburg (FSLG) (Bielecki et al., 1989; vanRossum et al., 1997) and closely related phase modulated Lee–Goldburg (PMLG) techniques (Vinogradov et al., 1999; Vinogradov et al., 2001) provide the shortest cycle times by far. This is very likely the reason that these methods presently provide the highest resolution that can be routinely achieved in ^{1}H solid state NMR (ssNMR) spectra. In model compounds ^{1}H resonances with line widths of only 100–200 Hz are routinely obtained.

Another approach to improving ^{1}H spectral resolution in ssNMR is to dilute the ^{1}H pool by extensive deuteration, and to use MAS alone as a line narrowing technique (McDermott et al., 1992). When combined with heteronuclear decoupling, the ^{1}H line widths observed in HETCOR spectra for model amino acids and peptides can also be made quite narrow, reportedly 0.2 ppm (Reif et al., 2001). Extensive dilution of the ^{1}H pool in general however also greatly reduces ^{1}H sensitivity. For protein NMR this is not a problem as the resonances of most interest are the amides. In this instance the protein can be perdeuterated, while the amides can subsequently be back-exchanged in normal water, retaining full ^{1}H sensitivity for these sites (Reif et al., 2003).

A key ingredient in solution phase protein NMR studies is the ^{1}H–^{15}N shift correlation map. Dispersion in this spectrum is key to sequential assignment and obtaining most NOE distance restraints. In addition, ^{15}N and ^{1}H chemical shifts are known to be extremely sensitive to structure, and appear to have potential for structure refinement (Neal et al., 2003). Recently single site resolution has been demonstrated in the ^{1}H–^{15}N correlation spectrum for two small proteins, the α-spectrin SH3 domain (van Rossum et al., 2003; Chevelkov et al., 2003) and ubiquitin (Paulson et al., 2003). In this paper we critically compare the resolution that can be obtained using combinations of FSLG, magnetic dilution, fast MAS and ^{15}N decoupling as the line narrowing techniques, with nanocrystalline ubiquitin in either ^{15}N enriched, or ^{2}H–^{15}N enriched form. Operating on an 800 MHz NMR instrument, the best resolution obtained is for perdeuterated material using MAS at 20 kHz and low power WALTZ-16 ^{15}N decoupling. In this instance the average ^{1}H line widths are only 0.26 ppm, with many as narrow as 0.17 ppm. The high resolution, ease of experimental setup, and the reduced RF power requirements make this technique very attractive for solid state ^{1}H NMR studies of proteins.

Experimental outline

Several factors influence the ^{1}H line widths obtained in the two dimensional ^{1}H–^{15}N correlation spectrum of a nanocrystalline protein. Foremost is the quality of the ^{1}H homonuclear decoupling. In this study we compare experiments employing FSLG decoupling to those with MAS alone for ubiquitin samples where the protein is either perprotio or perdeuterated and back-exchanged in normal water. Since the RF power applied is quite different for these two experiments, one should be cautious in simply comparing results with FSLG decoupling on and off. Two effects are of principal concern. First, the ^{1}H resolution and signal to noise in the indirect dimension critically depends upon the ^{1}H–^{15}N polarization transfer step. If the CP match drifts progressively further from the optimal condition as t_1 increases, the ^{1}H resolution will be degraded due to the decay of the ^{15}N signal. It is even possible for the resolution to be artificially enhanced if the tuning drifts so that the CP match gets better. Secondly, the ^{15}N line shape also indirectly perturbs the apparent ^{1}H resolution. Any overlap in the ^{15}N dimension will make the ^{1}H line widths measured from slices in the 2D spectrum appear greater. Therefore any change in the efficiency of the ^{1}H decoupling can also affect the apparent ^{1}H resolution. In light of these concerns the relative merits of different ^{1}H–^{15}N cross polarization (CP) conditions and transferred echo double resonance (TEDOR) (Schnell et al., 2001; Hing et al., 1992) transfers were studied, as well as the stability and line-narrowing performance of TPPM and XiX ^{1}H decoupling (Detken et al.,

2002). We also explore the efficacy of different types of ^{15}N decoupling during the ^{1}H evolution. The resolution obtained in different 2D ^{1}H–^{15}N HETCOR spectra is characterized by the distributions of ^{1}H and ^{15}N line widths obtained.

Pulse sequence design

Switching the carrier frequency $\pm\Delta\omega$ in FSLG decoupling can be accomplished by an actual frequency jump, or by linearly ramping the RF phase, in which case $\pm\, d\phi/dt = \pm\Delta\omega$. Which method is preferable depends exactly on how the RF is controlled and the inescapable timing delays in the response of the RF electronics to the control signals. In our experience these timing issues on both Varian and Chemagnetics instruments are simpler to handle when phase modulation is used. Implementation of FSLG decoupling by small discrete phase changes is indeed the same as the phase modulated Lee–Goldburg or PMLG-*n* sequences of S. Vega and co-workers with large *n*. As long as *n* is sufficiently large, there is no significant difference in the RF waveform produced by the two approaches. Therefore, in the phase ramped case when $n > 15$ we refer to this homonuclear decoupling method also as FSLG. The acronym PMLG will be reserved for when it is easier to discuss the RF waveform in terms of phase modulation, or if it is important to denote the number of phase steps *n* employed in each 2π pulse.

In this paper we introduce a modified version of the FSLG HETCOR method which deals with the effects of phase transients. We refer to this sequence, diagrammed in Figure 1, as the frequency jumped FSLG HETCOR pulse sequence (fj-FSLG or fj-PMLG). During t_1 the FSLG decoupling is implemented in the phase modulated fashion, stepping the phase a fixed increment every 250 ns, the minimum reliable time slice Δt for our timing generator. If the PMLG pulses are to be 2π nutations about the Lee–Goldburg (LG) field axis, only a few $\Delta\phi$ values can be chosen, since the number of phase steps in a PMLG 2π is simply $360/(\sqrt{3}\Delta\varphi)$. The resolution of our phase shifter is 0.25°, making 8° and 9° convenient phase steps. These choices result in 360.3° and 358.6° nutation angles respectively when the RF field angle is set to the magic angle condition. Once Δt is chosen the resonance offset is $\Delta\phi/\Delta t$, which also fixes the required RF field amplitude to $\sqrt{2}\Delta\varphi/\Delta t$. This corresponds to RF fields of amplitude $\omega_1^H/2\pi$ of 125.7 kHz for an 8° phase step, or 141.4 kHz for a 9° phase step (PMLG-26 and PMLG-23 respectively).

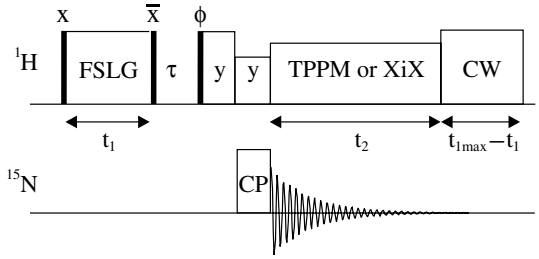

Figure 1. fj-FSLG pulse sequence. The solid black bars represent 90° pulses, labeled by the corresponding phase of the applied RF. The delay $\tau = 10$ μs is required to permit the synthesizer to stabilize after the frequency jump. The phase ϕ is cycled as $x,\bar{x}$ along with the receiver for spin–temperature alternation. A 10 μs spin locking field is applied on the ^{1}H channel prior to the cross polarization period at the power of the 90° pulse.

To avoid problems with the location of spinning side bands in the ^{1}H dimension, the dwell time in t_1 is most conveniently set close to the MAS rate ω_r. This in turn requires that an integer number of pairs of 2π nutations about the LG field vector fit into a rotor period. For a wide variety of model compounds using ^{1}H RF fields of 125 kHz or more in amplitude, we have found no degradation in resolution spinning well over 20 kHz. At our field strength a spin rate of 17–20 kHz then is convenient, accommodating four or five pairs of 2π FSLG pulses per rotor cycle with 8° or 9° phase steps. The instance where four pairs of 2π pulses occur per rotor period is known to result in a severe degradation in ^{1}H resolution because of interference effects (Vinogradov et al., 2001). Setting the MAS rate to 20 kHz instead of the synchronous 19,230 Hz value for PMLG-26 is a sufficient offset to avoid this and still minimize problems from spinning sidebands.

In the fj-PMLG implementation the ^{1}H magnetization is tipped into the xy plane by a $\pi/2$ pulse, and the FSLG decoupling commenced using RF of the same initial phase. For discussion purposes this is arbitrarily chosen here as x phase. At the end of t_1 the FSLG waveform has accumulated a net phase change of 180°, thus ending at $\bar{x}$. A final $\pi/2$ pulse of the same phase will flip the component of the magnetization along $\bar{y}$ to the

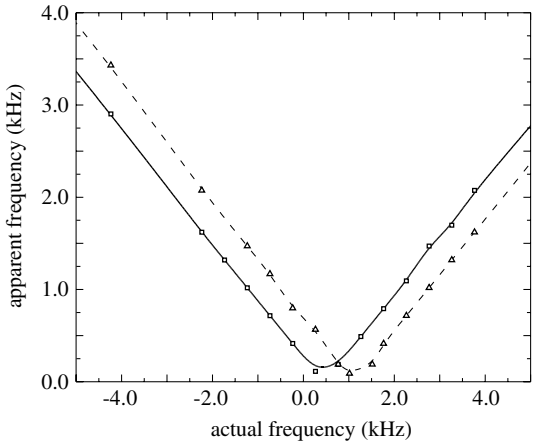

Figure 2. Apparent frequency vs. actual resonance offset for the adamantane ^{1}H resonance during FSLG. The data shown were taken with the probe tuned for minimum reflected power (squares, solid line), and with a 5% mismatch (triangles, dashed line). Direct ^{1}H detection was used. The pulse sequence employed is that portion of the sequence applied to the ^{1}H as shown in Figure 1 up to and including the pulse of phase ϕ.

z-axis. With an ideal spectrometer the first $\pi/2$ pulse starts the magnetization out orthogonal to the LG field, and the final $\pi/2$ pulse picks out the cosine modulated component of the ^{1}H magnetization for subsequent transfer to the ^{15}N for later detection. On a real spectrometer there are delays between the pulse program timing and when the RF actually shifts phase. The particular sequence used here makes compensation for these delays simply a matter of adjusting the precise lengths of the flip down and flip up pulses bracketing the FSLG evolution in t_1.

In addition, this arrangement is useful for dealing with the effects of phase transients (Vega, 2004). Just as in multiple pulse homonuclear decoupling schemes, the presence of phase transients at each step in the FSLG or PMLG waveform leads to an error term in the average Hamiltonian that produces an additional frequency offset (Rhim et al., 1973, 1974). The size of the effect can be appreciated from the scaling factor plot in Figure 2, where the apparent frequency of the adamantane ^{1}H resonance is plotted as a function of the actual resonance offset. For an ideal spectrometer the slope is the FSLG chemical shift scaling factor $1/\sqrt{3}$, and the intercept would be zero. The presence of phase transients in this particular example gives rise to a fixed offset the order of 500–1000 Hz. The size of the offset is sensitive to probe and amplifier tuning, and can limit the resolution attained if close attention is not paid to instrument stability. Also important to recognize is the fact that close to the minimum offset, the scaling plot is no longer linear. This is a well-known problem in multiple pulse homonuclear ^{1}H NMR. The usual solution is to always place the carrier to one side of the spectral window to ensure that the shift scale obtained is linear as desired. Quadrature detection schemes in t_1 are then not particularly useful. Performing the PMLG or FSLG with the carrier frequency set off resonance also helps suppress any additional error Hamiltonians that may be present which act as fields perpendicular to the LG vector, commonly known as second averaging. Recently this has been shown to also improve PMLG line narrowing in the presence of RF inhomogeneity (Vega, 2004).

The optimum carrier frequency of the RF for FSLG during t_1 and later for decoupling during t_2 will often be different. The fj-FSLG pulse sequence enables this frequency jump by taking the evolution during FSLG and projecting it first onto the z-axis where it can be stored while the ^{1}H frequency synthesizer is jumped to the optimum value for CP and decoupling. After a suitably short delay τ for the frequency jump, the ^{1}H magnetization can be spinlocked for CP transfer to ^{15}N, and the ^{15}N spectrum observed using TPPM or XiX decoupling. To keep the probe temperature constant the sequence ends with a final period of ^{1}H irradiation of length $t_{1\max} - t_1$. This keeps the applied power constant for all values of t_1, important for holding the probe tuning constant. As just discussed, since the phase transients are largely determined by the probe tuning, a drift in the probe tuning over the experiment time will result in the apparent carrier frequency drifting in t_1. The most serious effect of such drift is degradation in the ultimate ^{1}H resolution that can be achieved.

Alternatively, the ^{1}H homonuclear dipolar couplings may be suppressed by isotopic dilution of the ^{1}Hs in combination with fast MAS. For detection of backbone amides of a protein, this is easily achieved with a perdeuterated sample back-exchanged in normal water. For comparison to the FSLG homonuclear decoupled spectra, ^{1}H–^{15}N HETCOR spectra with free ^{1}H evolution under MAS were acquired by simply inserting a t_1

delay between the initial ^{1}H $\pi/2$ pulse and the spinlock used in the CP transfer.

Methods and materials

Sample preparation

Two types of samples have been studied in this work. P-form ubiquitin nanocrystals were prepared using polyethylene glycol (PEG) as a crowding agent and a centrifugal evaporator as described elsewhere (Martin and Zilm, 2003). M-form crystals are obtained using 2-methyl-2,4-pentanediol (MPD) as a precipitating agent. These were prepared by adding one aliquot ubiquitin stock solution (25 mg/ml ubiquitin in 20 mM sodium citrate pH 4.1) to 1.5 aliquots of d_{12}-MPD. The solution was stored at 4 °C overnight to allow ample time for precipitation to occur (Igumenova, 2003). Four mg of wet nanocrystalline protein were transferred to 2.5 mm outer diameter zirconia rotors having Kel-F sample spacers fitted with fluorosilicon o-rings to prevent protein dehydration. The inner surface of the MAS rotor was also coated with a film of fluorolube wax (Halocarbon 1500, Halocarbon Products Corp.). Protein samples prepared in this manner are stable for many months. The results obtained for both preparations were quite similar, and for brevity only those for M-form crystals are reported on in significant detail.

Ubiquitin enriched solely in ^{15}N was provided by VLI Research Inc. salt free, and could be used without further purification. Perdeuterated ^{15}N enriched ubiquitin was prepared in *E.coli* BL21star cells using a plasmid obtained from Prof. Tracy Handel, U.C. Berkeley. The cells were grown in M9 minimal media containing 1 g/l $^{15}NH_4Cl$ and 2 g/l U-D_6-glucose made in 98% D_2O. Isotopically enriched compounds were obtained from Cambridge Isotope Laboratories, Inc. This protein was purified using reversed phase HPLC and the identity and isotope incorporation was confirmed using electrospray mass spectrometry.

NMR spectroscopy

All data presented in this study were collected at a sample temperature of ~2 °C using a Varian INOVA NMR spectrometer operating at 799.6 MHz for ^{1}H and equipped with a home-built $^{1}H/^{13}C/^{15}N$ triple resonance probe that has previously been described in detail (Martin et al., 2003; Martin and Zilm, 2004). ^{1}H chemical shifts were referenced to external DSS by measuring the adamantane methylene and methine ^{13}C resonance frequencies and using the Ξ ratio published elsewhere (Morcombe and Zilm, 2003). The ^{15}N zero frequency was then set to liquid NH_3 using the recommended Ξ ratio of 10.1329118% (Markley et al., 1998). Field drift was compensated for by computer control of the room temperature B_o coil.

^{15}N spectroscopy was optimized on the protein samples of interest. Both the CP matching condition and the decoupling modulation parameters are found to be too sensitive to simply be set on a secondary standard. Sufficiently reproducible CP transfer at a MAS rate of 20 kHz was obtained only after much effort was put into stabilizing the output of the ^{15}N power amplifier (American Microwave Technologies model 3200B or 3304C). Noise blanking was kept to the minimum to keep the amplifier in a more stable thermal state. It was also found that utilizing the lowest ^{15}N power level consistent with the chosen MAS rate helped with thermal stability. Without these precautions the output power is observed to drift the order of ± 0.2 dB on the time scale of tens of minutes to a few hours. Constant power level CP transfers resulted in a larger signal than ramped CP transfers, with a 150 μs contact time being optimal for amides. Spectra obtained using a match where ω_1^H was set to $\omega_1^N + \omega_r$ also displayed the most uniform polarization transfer profile across the entire spectrum. These results are expected to be quite dependent on the level of RF homogeneity provided by the probe (Martin et al., 2003). The CP enhancement obtained is 4.5, determined by an inversion recovery T_1 experiment initiated by CP and an immediate flip down of the ^{15}N magnetization to the $-z$-axis. The average ^{15}N T_1 was also determined in this experiment to be 24 s.

TEDOR transfers were also investigated, with a cycle of 2 rotor periods found optimum for amides at the 20 kHz MAS rate. A comparison of CP and TEDOR enhancement vs. RF field is shown in Figure 3. While TEDOR transfer is much more stable for a larger deviation from the optimal applied power, it does provide about 30%

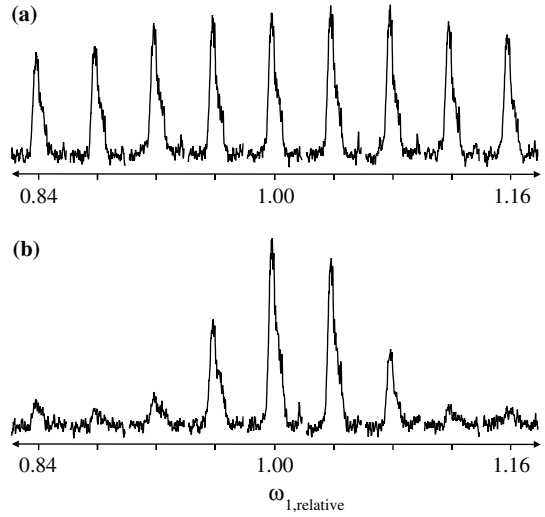

Figure 3. Sensitivity of polarization transfer efficiency to ^{1}H RF field strength setting in (a) TEDOR and (b) CP ^{1}H to ^{15}N transfers with 20 kHz MAS in P-form ubiquitin. Arrays of ^{15}N spectra are depicted as a function of the ^{1}H RF field amplitude. The range of ^{1}H power level spanned is one-third of the optimum RF amplitude, centered about the optimum value, with the RF field strength varying linearly in either direction. In each case 16 scans were acquired, the spectra were zero filled twice, and apodized with 50 Hz of line broadening. All spectra are plotted on the same vertical scale. The 90° pulse widths were 4.5 μs for the ^{15}N and 2.2 μs for the ^{1}H in the TEDOR experiment.

less signal under these conditions, and for this reason CP was used instead in this particular study. Increased spinning speed further improves TEDOR transfer (Schnell et al., 2001), and we have observed at spinning speeds over 28 kHz that the insensitivity of TEDOR to RF homogeneity makes it superior to CP for amide ^{1}H to ^{15}N transfers.

Both TPPM (Bennett et al., 1995) and XiX (Detken et al., 2002) decoupling were used in this study. The adjustment of TPPM for optimum performance is sufficiently delicate that it is always optimized on the protein sample itself. Even though XiX was found to provide more stable decoupling, TPPM could be carefully adjusted to give somewhat improved performance. While there are reasons to expect decoupling of ^{1}H from ^{15}N to be difficult in some instances (Ernst et al., 1996), the source of the sensitivity of the ^{15}N resolution to the decoupling parameters and the variability observed between the different amide sites remains an open question.

FSLG HETCOR experiments used the fj-FSLG pulse sequence in Figure 1 with 8° steps. The ^{1}H carrier is set to ~8 ppm for decoupling during t_2, and jumped 6 kHz lower in frequency for the FSLG decoupling during t_1. Resolution is optimized by adjusting this resonance offset, using a $^{13}C_2$–^{15}N enriched glycine sample and recording a ^{1}H–^{13}C HETCOR. The sample used is of crystal form-b (Kimura et al., 1998), and the splitting of the diastereotopic ^{1}Hs in the ^{1}H spectrum is used to judge the quality of the ^{1}H–^{1}H decoupling. The lengths of the ^{1}H 90° pulses bracketing the FSLG decoupling are empirically adjusted to minimize zero frequency and phasing artifacts in the indirectly detected ^{1}H dimension. Referencing of ^{1}H chemical shifts and determination of the FSLG scaling factor was accomplished by comparison to a HETCOR taken without FSLG line narrowing (vide infra).

T_2 measurements were performed on M-form ubiquitin samples. ^{15}N T_2s were determined using a rotor synchronized spin echo following the ^{1}H–^{15}N CP transfer. ^{1}H T_2s were measured by a rotor synchronous $(\frac{\pi}{2})_x - \tau - (\pi)_y - \tau$ spin echo sequence applied to the ^{1}H prior to turning on the y-phase ^{1}H spinlocking RF field for CP to ^{15}N. Both the ^{15}N and ^{1}H T_2 measurements using Hahn echoes were performed at MAS rates of 10 and 20 kHz. The ^{1}H measurements were repeated with and without simultaneous application of a ^{15}N π pulse with the ^{1}H π pulse. With the MAS rate set to 20 kHz additional ^{1}H T_2 measurements were made with a train of rotor-synchronous xy phase alternated π ^{15}N pulses (Gullion et al., 1990) to the ^{15}N for decoupling (RSPI decoupling) during the ^{1}H evolution.

^{15}N decoupling efficacy was ultimately assessed by comparing four two-dimensional ^{1}H–^{15}N correlation spectra differing in the mode of ^{15}N decoupling. The first used free evolution, the second a single 9 μs long ^{15}N π pulse midway through t_1 and the third RSPI ^{15}N decoupling. The final spectrum was obtained with WALTZ-16 decoupling where the ^{15}N RF field amplitude $\omega_1^N/2\pi$ had been set at 11 kHz. Each data set was acquired in 4.75 h, and worked up with zero filling twice in the ^{15}N and ^{1}H dimensions. Baseline corrections were performed, but no weighting functions were applied. Line widths were determined for 23 individual peaks that could be easily resolved in both the ^{15}N and ^{1}H dimensions in all four spectra.

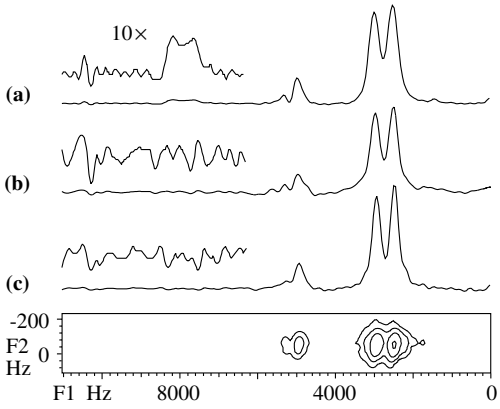

Figure 4. Effect of broadband ^{13}C decoupling during ^{1}H evolution in the FSLG experiment. Spectra shown are skyline projections of 2D ^{1}H–^{13}C HETCOR spectra. The sample used is 1,2–^{13}C labeled glycine, and the MAS frequency set to ~19 kHz. (a) no ^{13}C decoupling employed during the evolution, (b) GARP decoupling, and (c) WALTZ-16 decoupling. The ^{13}C decoupling amplitude $\omega_1^C/2\pi = 2.5$ kHz. The inserts depict 10× vertical expansions to indicate the t_1 noise levels. In (a) where no ^{13}C decoupling was used, the noise level is substantially less than in (b) or (c).

Comparison of ^{1}H MAS resolution obtained by FSLG, magnetic dilution and ^{15}N decoupling

In acquiring FSLG HETCOR spectra no ^{15}N decoupling has been applied. The reason for this can be appreciated by reference to Figure 4 depicting ^{1}H–^{13}C FSLG HETCOR spectra for our standard glycine sample. The three skyline projections differ only in the type of ^{13}C decoupling used. GARP decoupling has little effect on the resolution, while WALTZ-16 produces a small but measurable line narrowing. However, this narrowing is not worth the price paid in sensitivity. While not obvious from the projections themselves, the 10 × vertical expansion of the noise shown for each trace makes clear the significant increase in t_1 noise that accompanies ^{13}C decoupling in comparison to no ^{13}C decoupling at all. This t_1 noise may be due to small amounts of CP transfer occurring during t_1 while both RF fields are present (Ishii et al., 1995) or interference with the MAS averaging of the ^{1}H–^{13}C dipolar coupling. Given this problem, simultaneous application of FSLG and broadband ^{15}N decoupling was not used in this study on protein samples.

^{1}H–^{15}N correlation spectra were acquired for both perprotio and back-exchanged perdeutero P-form ubiquitin samples at a MAS rate of 20 kHz. In FSLG experiments the resolution obtained for the perdeuterated samples was slightly better, indicating that deuterium decoupling by MAS alone was sufficient. With this crystal polymorph the peaks in the ^{1}H–^{15}N map are doubled due to fact that there are two molecules in the asymmetric unit. In light of this all further comparisons were made using perdeuterated back-exchanged M-form samples, as there is only one molecule in the M-form crystal asymmetric unit. This reduces the congestion in the spectra obtained and makes comparison of line widths much more straightforward.

Figure 5 compares ^{1}H–^{15}N HETCOR spectra obtained for the perdeuterated M-form crystals at different spin rates using either the fj-FSLG sequence or MAS with RSPI ^{15}N decoupling. The lack of any measurable t_1 noise in the spectra shown attests to the effectiveness of the approach used here to stabilize magnetization transfer and probe tuning. The spectra in the left hand column (a1)–(c1) were obtained using FSLG decoupling at $\omega_r/2\pi = 20.0$, 15.384 and 10.989 kHz. In all cases the FSLG 2π time was 6.5 μs, resulting in five pairs of 2π pulses and seven pairs of 2π pulses respectively per rotor period for the 15.384 and 10.989 kHz results. In these cases the FSLG modulation was approximately synchronous with the MAS. The next higher spin rate at 20 kHz was chosen to avoid the 4 pairs of 2π pulses per rotor period condition (19.230 kHz) where MAS averaging and FSLG decoupling interfere. As judged from the contour plots provided, the resolution improves steadily with increasing MAS rate. The presence of the well resolved outlying peaks makes it possible to reference these spectra and determine the FSLG scaling factor (0.58) by direct comparison to the data obtained without FSLG decoupling.

The spectra in Figure 5(a2)–(c2) make the same spinning speed comparison using MAS alone for ^{1}H homonuclear decoupling and RSPI ^{15}N decoupling. As the contour plots show there is a much stronger dependence on MAS rate in this instance as expected. Although the ^{1}H lines are broader in Hz, the chemical shift is not scaled as in the FSLG method. On a ppm scale the ^{1}H lines eventually become narrower in width than those obtained by FSLG decoupling at the highest spin rate.

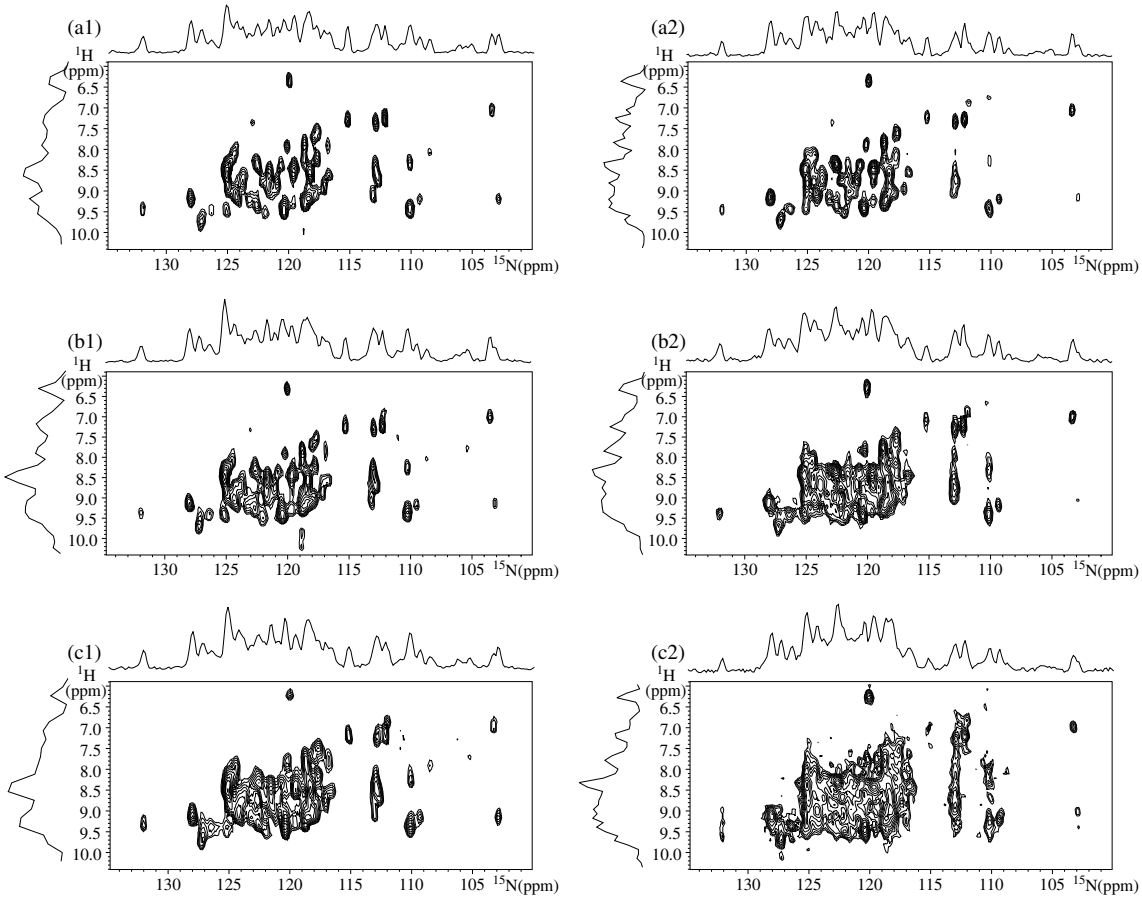

Figure 5. Spinning speed dependence of ^{1}H–^{15}N HETCOR spectra for M-form ubiquitin taken using (a1)–(c1) the fj-FSLG method or (a2)–(c2) with MAS for ^{1}H homonuclear line narrowing and RSPI ^{15}N decoupling. The FSLG spectra were referenced and scaled by comparing the spectrum in (a1) to that in (a2). MAS speeds (a) 20 kHz and (b) 15.384 kHz and (c) 10.989 kHz. Each spectrum used 2 h of data acquisition and a 20 ms ^{15}N chemical shift evolution period. The ^{1}H evolution was set as close as practical to 6 ms for the spectra taken with FSLG homonuclear decoupling, and restricted to 4 ms for the spectra taken using only MAS and ^{15}N decoupling. This was done to provide for equivalent chemical shift evolution taking into account the FSLG scaling factor of $1/\sqrt{3}$. The data were zero filled twice in both t_1 and t_2, and no apodization functions were applied. ^{1}H TPPM decoupling with $\gamma B_1/2\pi = 98$ kHz was applied during ^{15}N detection. The vertical scale was adjusted to keep the average height of five peaks (A47, I36, Y59, S20 and G46) constant. The pertinent parameters for each spectrum are as follows: (a1) MAS at 20 kHz, FSLG during t_1, dwell in $t_1 = 52$ μs, 120 t_1 points for a total acquisition time t_{1acq} of 6.1 ms in the indirect dimension. (a2) no FSLG, MAS at 20 kHz, dwell in $t_1 = 100$ μs, 40 t_1 points acquired for a total acquisition time t_{1acq} of 3.9 ms in the indirect dimension. (b1) MAS at 15.384 kHz, FSLG during t_1, dwell in $t_1 = 65$ μs, 96 t_1 points for a total acquisition time t_{1acq} of 6.2 ms in the indirect dimension. (b2) no FSLG, MAS at 15.384 kHz, dwell in $t_1 = 130$ μs, 32 t_1 points acquired for a total acquisition time t_{1acq} of 4.2 ms in the indirect dimension. (c1) MAS at 10.989 kHz, FSLG during t_1, dwell in $t_1 = 91$ μs, 68 t_1 points for a total acquisition time t_{1acq} of 6.2 ms in the indirect dimension. (c2) no FSLG, MAS at 10.989 kHz, dwell in $t_1 = 182$ μs, 24 t_1 points acquired for a total acquisition time t_{1acq} of 4.3 ms in the indirect dimension.

T_2, ^{15}N decoupling and line width measurements

It is difficult to judge the true ^{1}H resolution from the contour maps alone as they are more indicative of the line shapes towards the base of larger peaks. The distribution of ^{1}H line widths is more informative in this instance when evaluating the efficacy of different decoupling techniques, since it is quite easy to convince oneself that a method is ineffective by focusing one's attention on the wrong resonance. To this end the ^{1}H and ^{15}N T_2 decays were investigated as described earlier in experiments where only MAS was used for ^{1}H homonuclear decoupling.

The entire amide band was integrated for ^{15}N T_2 data, and the signal decays fit well to a single

exponential. These fits yielded ^{15}N T_2 values of 24.3 ms at 20 kHz and 26.5 ms at 10 kHz, corresponding to refocusable line widths of 13 Hz or less. The slight shortening in T_2 as the spin rate increases is most probably due to a decrease in the efficacy of the XiX decoupling, a consequence of the ^1H RF field at 100 kHz being only about five times this higher MAS rate. Presumably this could be improved upon with an increase in decoupling power, if not for concerns about sample damage due to RF heating. In either case the ^{15}N T_2 accounts for less than half the average ^{15}N line width observed (0.5 ppm, vide infra).

^1H T_2s are much more dramatically affected by spinning speed. Initial experiments used a single rotor synchronous ^1H π pulse for refocusing the magnetization, and WALTZ-16 decoupling with $\omega_1^N/2\pi = 2.5$ kHz during the transverse dephasing delay. The decays for the net ^1H magnetization observed do not fit single exponential curves particularly well, nevertheless the effective T_2 values obtained in this manner provide a concise description of the results. At 10 kHz the average ^1H T_2 was found to be $\sim$0.34 ms, whereas at 20 kHz the ^1H T_2 lengthened to $\sim$1.52 ms. Two dimensional ^1H–^{15}N HETCOR spectra with this level of WALTZ-16 decoupling were also acquired at these two spin rates for comparison, and in general displayed enhanced resolution at the higher spin rate. However, the degree of narrowing obtained is not uniform across the spectrum.

The uneven performance of low level WALTZ-16 ^{15}N decoupling and our previous observation that a ^{15}N π pulse midway through t_1 was ineffective as a decoupling technique for P-form samples suggested that additional T_2 measurements might prove informative. These were performed on a perdeuterated back-exchanged M-form sample with 20 kHz MAS using several different ^{15}N decoupling schemes. In every instance spin echoes were made synchronous with the sample rotation. The decays observed again were decidedly non-exponential, and now so much so that fits to single exponential curves were not particularly useful. Applying simultaneous ^1H and ^{15}N π pulses after an integral number of rotor periods refocuses only the ^1H chemical shift and resulted in the most rapid echo decay, with an effective T_2 of about 1 ms. If the ^{15}N π pulse is eliminated this decay measurably lengthens. Adding a train of rotor synchronous ^{15}N π pulses before and after the ^1H refocusing π pulse lengthens the echo decay further still, almost by a factor of two. Given the significant dispersion displayed in the T_2 relaxation of the net ^1H magnetization, a more useful approach is to examine the distribution of line widths obtained in ^1H–^{15}N HETCOR spectra with different modes of ^{15}N decoupling.

The resolution provided by the M-form samples is sufficient to identify 23 resonances which have no significant overlap with other peaks in either the ^{15}N or the ^1H dimensions, and are known on the basis of other work (Morcombe) to correspond to single amide sites. Spectra were acquired with no ^{15}N decoupling, with a single ^{15}N π pulse midway through t_1, and with a train of rotor-synchronous ^{15}N π pulses. Since it had been observed that WALTZ-16 decoupling with $\omega_1^N/2\pi$ set to 2.5 kHz provided mixed results, a spectrum was acquired where this RF amplitude was increased to 11 kHz. This value was chosen to reduce the WALTZ-16 cycle time while at the same time remaining low enough to avoid interference with the 20 kHz MAS. WALTZ-16 decoupling at this level is also still a factor of 4.5 less in average applied power than the train of rotor synchronized 9.0 μs long π pulses, and should therefore be less taxing on both the probe and the sample. For comparison a high resolution FSLG spectrum was also acquired on the same sample.

Example high resolution ^1H–^{15}N HETCOR spectra used in these comparisons are shown in Figure 6. Assignments of the amide peaks, which will be reported on at a later date, are indicated on the spectrum obtained using MAS and ^{15}N decoupling. Nearly all peaks appear in both HETCOR spectra, which principally differ in the ^1H line widths observed. For a small subset of the peaks there is a noticeable variability in the intensities, most clearly judged by reference to the skyline projection plotted at the top of each 2D map representing the ^{15}N spectrum. A few of these are amide peaks which also appear to be difficult to cross polarize, presumably because of large amplitude molecular motions. Additional variable intensity peaks are observed between 104 and 112 ppm in the ^{15}N dimension, some of which correspond to glutamine and arginine sidechain exchangeable protons. When a site has more than a single directly attached proton, FSLG is expected to work better as a homonuclear

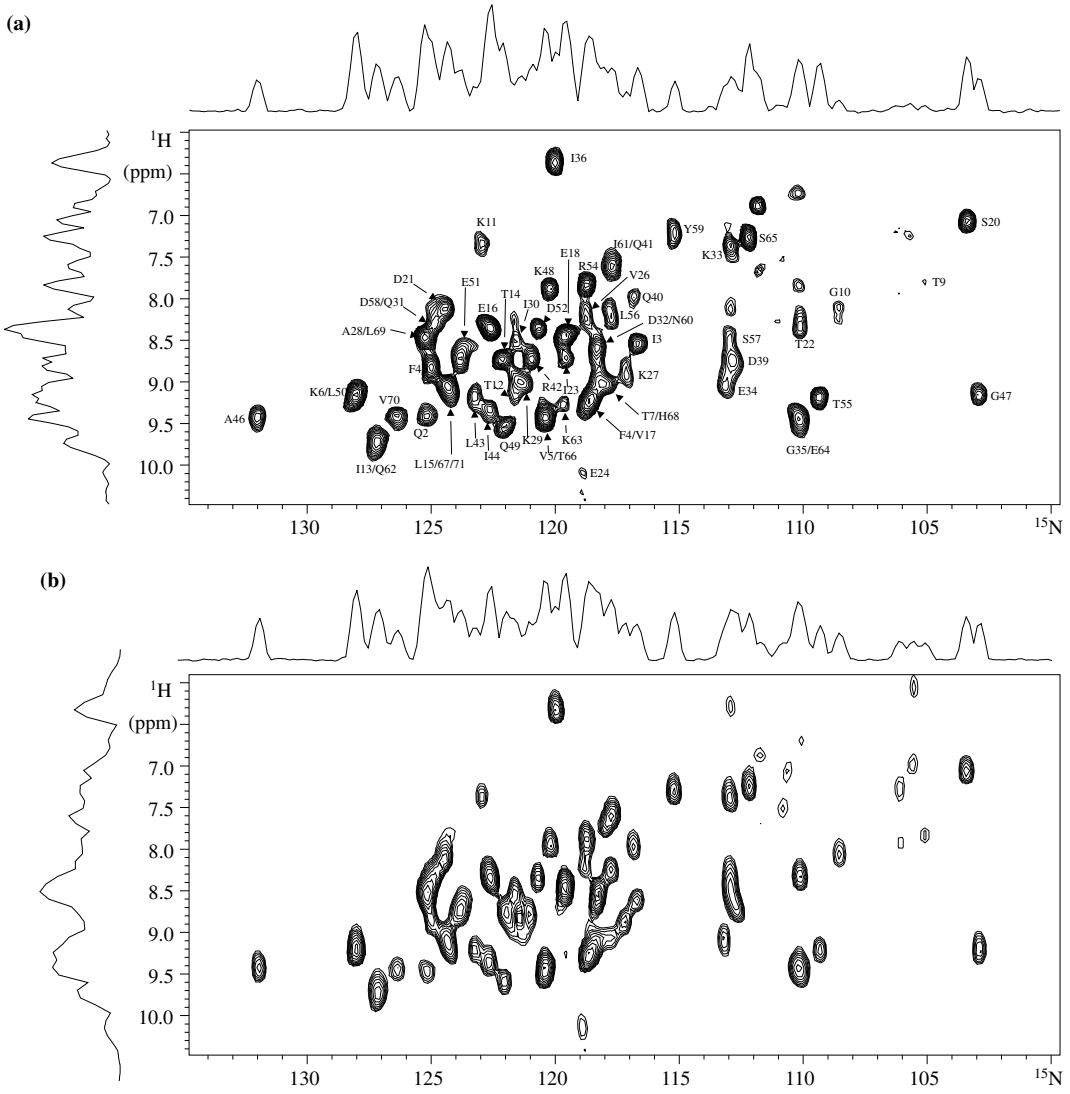

Figure 6. Comparison of ^{1}H–^{15}N correlation spectra taken (a) with RSPI ^{15}N decoupling and only MAS for ^{1}H homonuclear decoupling with (b) FSLG ^{1}H homonuclear decoupling and no ^{15}N decoupling. Both data sets used a 20 ms ^{15}N evolution time. In (a) 140 scans were acquired for 80 complex t_1 increments using a 2 s recycle delay. Total collection time in this case was 12.7 h. The ^{1}H evolution went out to 7.9 ms. In (b) 120 scans were taken for 192 increments with a 2 s recycle delay. The maximum ^{1}H evolution time was 9.9 ms, and the data collected over 13.1 h. No resonances are observed in either the ^{15}N or ^{13}C spectrum for residues in the loop consisting of residues 9–13 and for residues 72–76 in the C-terminus, most likely a result of extensive molecular mobility. All amide resonances outside these two regions are observed with the exception of those for residues G53 and N25.

decoupling technique than MAS alone. This would result in narrower and therefore more intense cross peaks in the FSLG spectrum. Other observed differences may be the result of molecular motion interfering with either the MAS or FSLG line narrowing. In this paper we will confine our attention to the backbone amides for the majority of the protein where molecular dynamics is not an issue.

Distributions of the observed ^{1}H line widths are plotted in Figure 7 for each type of ^{15}N decoupling used. As a control the ^{15}N line width distributions were also determined (not shown). These did not depend upon the mode of ^{15}N decoupling used during t_1 as expected. The average observed ^{15}N line width is $\sim$0.5 ppm with a standard deviation of $\sim$0.1 ppm for this sample when XiX decoupling with $\omega_1^H/2\pi$ set to 100 kHz is used.

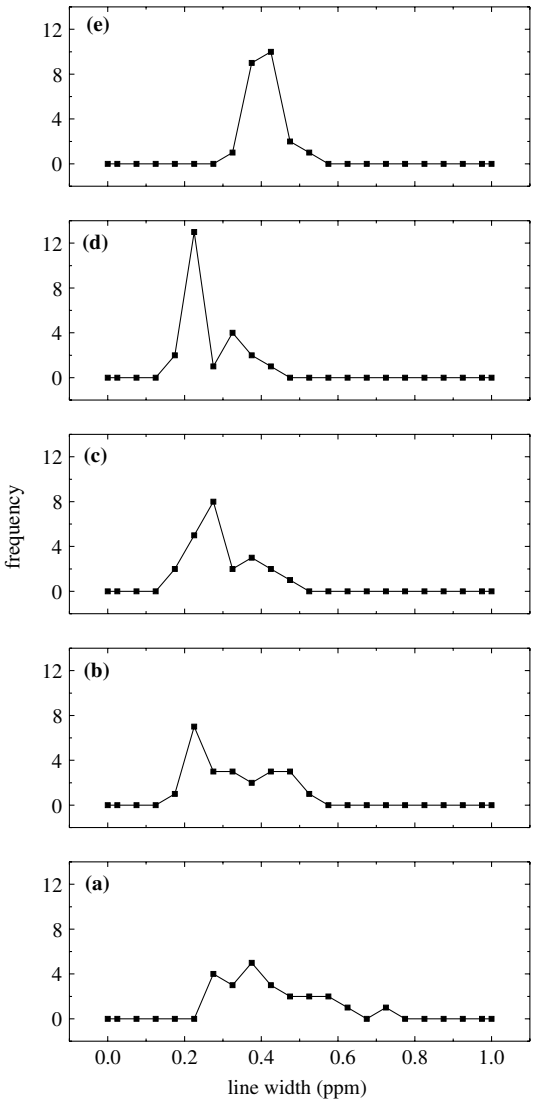

Figure 7. Effect of ^{15}N decoupling on the distribution of ^{1}H line widths observed in MAS ^{1}H–^{15}N HETCOR spectra of perdeuterated back-exchanged M-form ubiquitin. Line widths, taken as full width at half maximum, were measured for 23 peaks. Those chosen were sufficiently resolved in both the ^{1}H and ^{15}N dimensions so as not to require deconvolution of neighboring resonances. The specific resonances are for residues 2, 3, 16, 18, 20, 21, 27, 33, 36, 42, 43, 44, 46, 47, 48, 49, 51, 52, 55, 56, 59, 65 and 70. The line widths were sorted into bins of 0.05 ppm wide, resulting in the histograms depicted. For the distributions in (a)–(d) only MAS was used for ^{1}H line narrowing. In (a) no ^{15}N decoupling was applied, in (b) a single ^{15}N π pulse midway through t_1 was applied, in (c) RSPI ^{15}N decoupling was used and in (d) WALTZ-16 ^{15}N decoupling was applied with $\omega_1^N/2\pi = 11$ kHz. The distribution in (e) is obtained using FSLG for ^{1}H homonuclear decoupling without any form of ^{15}N decoupling.

In contrast, it is quite apparent that the ^{15}N decoupling has a significant effect on the observed ^{1}H resolution. The ^{1}H line width distributions obtained are depicted in Figure 7(a)–(e). These span a sizeable range of line widths and can be quite asymmetric, consistent with the non-exponential T_2 decays discussed earlier.

The broad distribution in Figure 7(a) was obtained when no ^{15}N decoupling is applied. Line widths (full width at half-maximum, fwhm) ranging from 0.27 to 0.75 ppm are observed, with the average falling at 0.43 ppm. Applying a single ^{15}N π pulse midway through t_1 for decoupling results in the distribution shown in Figure 7(b). The span of the distribution now narrows to cover 0.19–0.55 ppm, and the average line width has dropped to 0.33 ppm. While the resolution has improved on average, and the distribution shifted significantly lower, the narrowing obtained is not uniform. Some lines narrow dramatically while some do not narrow at all.

These data explain our earlier observation (Paulson et al., 2003) that a single ^{15}N π pulse appeared ineffective as a ^{15}N decoupling method in ^{1}H–^{15}N HETCOR spectra of P-form samples, while elsewhere the same approach in application to ^{1}H–^{13}C HETCOR spectroscopy (Lesage and Emsley, 2001) provided useful X-nucleus decoupling. In our P-form ubiquitin data only a few individual lines were well resolved enough and had high enough signal to noise to make dependable line shape measurements on. On closer inspection it is now clear that the apparent efficacy of this approach to X-nucleus decoupling depends on the particular lines observed. In the case of the P-form samples the most resolved lines just happen to be some of those which are not narrowed by this technique.

Additional insight into this behavior is provided by the next distribution shown in Figure 7(c). These line widths were obtained using RSPI ^{15}N decoupling. The minimum line width stays at 0.19 ppm, while the upper limit has dropped to 0.49 ppm, and the average has dropped an additional 0.04 ppm to 0.29 ppm. This result indicates that a dynamic process of some sort is interfering with the coherent refocusing of the ^{1}H–^{15}N scalar coupling interaction by a single π pulse. Applying π pulses at a rate more rapid than the time scale of this dynamic process provides for more efficient refocusing. The effect observed is

analogous to how a Carr-Purcell echo train provides for better refocusing of chemical shifts in the presence of chemical exchange. The most likely mechanism here is interference with any residual ^{1}H–^{1}H dipolar interaction. Since the homonuclear ^{1}H dipolar coupling does not commute with the heteronuclear ^{1}H–^{15}N dipolar or scalar coupling interactions, the heteronuclear portion of the propagator will not simply factor from the homonuclear portion. This is a necessary requirement for the scalar interaction to be refocused by a simple spin echo on the ^{15}N nuclei, or for the heteronuclear dipolar coupling to be coherently averaged to zero independently by MAS. However, as the echo period is made shorter and shorter, the non-commutation of these terms becomes less and less of a restriction in an average Hamiltonian sense. Therefore, the apparent T_2 lengthens when a train of rotor synchronized echoes is employed instead of a single pulse. The use of faster MAS rates, which will provide for a smaller residual ^{1}H–^{1}H dipolar interaction, may then make it much easier to attain more effective decoupling of the ^{1}H–^{15}N scalar interaction during t_1.

Switching to WALTZ-16 ^{15}N decoupling with $\omega_1^N/2\pi$ set to 11 kHz provides the ^{1}H line width distribution depicted in Figure 7(d). The minimum line width has been reduced to 0.17 ppm, and the maximum is no more than 0.41 ppm. The distribution is significantly more peaked at the narrow end of the distribution, as well as being more symmetric. With this decoupling scheme the average ^{1}H line width has dropped to 0.26 ppm, and the median line width is only 0.23 ppm.

The final distribution shown is obtained from a FSLG spectrum using parameters as listed in the caption. The distribution is the most symmetric obtained, and has an average of 0.4 ppm. It is interesting to note that removing the FSLG scaling factor, the average line width on a Hz scale at 190 Hz is essentially the same as the 210 Hz obtained using only MAS for homonuclear decoupling and WALTZ-16 for ^{15}N decoupling. Applying WALTZ-16 decoupling here is not practical as discussed earlier because of the resulting t_1 noise. The use of a π pulse midway through t_1 is also problematic as the FSLG has intentionally been made asynchronous with the MAS rotation to avoid interference affects, and the ^{15}N π pulse then would lead to dephasing due to ^{15}N shift anisotropy recoupling. Programming a train of rotor synchronous ^{15}N π pulses while at the same time having the FSLG asynchronous with the MAS rate is also not feasible with the hardware used in these experiments.

Conclusions

An investigation of the parameters affecting resolution in ^{1}H–^{15}N correlation spectroscopy of proteins has been performed at 800 MHz. ^{1}H resolution was explored using either FSLG or fast MAS combined with deuteration for ^{1}H homonuclear decoupling. Obtaining the best performance in any of the approaches studied required meticulous stabilization of both the polarization transfer and ^{1}H decoupling. With a carefully aligned instrument it was shown that 20 kHz MAS in conjunction with magnetic dilution suppressed the ^{1}H–^{1}H dipolar couplings as well as FSLG homonuclear decoupling did for deuterated ubiquitin. In addition to being a much simpler experiment to perform, the reduction in overall applied RF power makes this a much less risky experiment to apply to easily damaged protein samples.

Combining deuteration, 20 kHz MAS, and WALTZ-16 ^{15}N decoupling resulted in the most highly resolved ^{1}H–^{15}N correlation spectra with median ^{1}H line widths of only 0.23 ppm. These narrow ^{1}H line widths open the door to ^{1}H detection, as has already been reported on by ourselves (Paulson et al., 2003) as well as by Chevelkov et al. (2003). The present paper quantitatively reconciles the differences in resolution observed in these latter two pieces of work by demonstrating the marked dependence of the ^{1}H T_2 on the MAS rate ω_r. Even though the amide protons are fairly dilute in a perdeuterated protein sample, increasing the MAS rate from 10 to 20 kHz resulted in nearly a factor of 4.5 increase in the effective ^{1}H T_2.

Elimination of the need for FSLG or other homonuclear decoupling schemes also makes it practical to apply broadband ^{15}N decoupling during the ^{1}H evolution, providing for significant additional line narrowing. Transverse ^{1}H relaxation time measurements and a characterization of the line width distributions demonstrated that application of a single π pulse to the ^{15}N midway through t_1 provides less than optimal ^{15}N

decoupling. This is most likely a result of the fact that the residual ^1H–^1H dipolar interaction does not commute with the ^1H–^{15}N scalar or dipolar Hamiltonians. While a quantitative description of the residual line broadening is a topic of ongoing research, it is clear that improved ^{15}N decoupling should be obtained at higher ω_r. Determining the distribution of ^1H line widths proved to be the most informative approach to evaluating the efficacy of different decoupling techniques. It is quite easy to convince oneself that a method is ineffective by focusing one's attention on the wrong resonance.

Some applications are of course not compatible with deuteration, for instance resolution of side-chain ^1Hs, and then FSLG is still the method of choice. Experiments of this type will benefit from the approaches to long term instrument stabilization described here. The use of techniques such as WALTZ-16 for heteronuclear decoupling is not recommended in FSLG experiments if t_1 noise is to be avoided. In this instance the application of a single π pulse midway through t_1 is most likely the best approach to X-nucleus decoupling. The RSPI decoupling technique will usually not be convenient to apply unless the FSLG decoupling can also be performed synchronously with the MAS rotation.

It is very likely that a further increase in spinning speed beyond 20 kHz will provide additional improvement in the ^1H resolution by providing both better homonuclear and heteronuclear decoupling. This could be quite important, as the ability to further resolve individual resonances is a rapidly increasing function of the resolution in the present range of line width. If the 2D spectra here are taken as representative for small proteins, we see that the ^1H resonances span $\sim$4 ppm while the ^{15}N lines are contained within $\sim$32 ppm. Considering that the average ^1H lines are a factor of 2 narrower on a ppm scale, the overall resolution of the ^{15}N dimension is only approximately 4 times greater than that observed in the ^1H dimension. Since another 50% decrease in ^1H line width seems plausibly in reach, the dispersion in the ^1H dimension may come within a factor of two of that in the ^{15}N dimension. Taking advantage of higher MAS speeds will entail dealing with greater frictional heating, and likely require higher power ^1H decoupling if the resolution is not to decrease in the ^{15}N dimension. Such experiments are currently in progress and will be the subject of a future report.

Acknowledgements

The authors are grateful to Dr. Tauseef Butt, VLI Research, for the gift of a sample of ^{15}N enriched ubiquitin. KWZ would like to thank Dr. Alexander Vega for stimulating discussions on phase transients and sharing a manuscript on phase transients in PMLG spectroscopy prior to submission. This work was supported in part by grants from the National Science Foundation and the Wm. M. Keck Foundation and by Yale University. CRM gratefully acknowledges the support of a NSERC post-graduate fellowship.

References

Bennett, A.E., Rienstra, C.M., Auger, M., Lakshmi, K.V. and Griffin, R.G. (1995) *J. Chem. Phys.*, **103**, 6951–6958.

Bielecki, A., Kolbert, A.C. and Levitt, M.H. (1989) *Chem. Phys. Lett.*, **155**, 341–346.

Bronnimann, C.E., Hawkins, B.L., Zhang, M. and Maciel, G.E. (1988) *Anal. Chem.*, **60**, 1743–1750.

Chevelkov, V., Rossum, B.J., Castellani, F., Rehbein, K., Diehl, A., Hohwy, M., Steuernagel, S., Engelke, F., Oschkinat, H. and Reif, B. (2003) *J. Am. Chem. Soc.*, **125**, 7788–7789.

Detken, A., Hardy, E.H., Ernst, M. and Meier, B.H. (2002) *Chem. Phys. Lett.*, **356**, 298–304.

Ernst, M., Bush, S., Kolbert, A.C. and Pines, A. (1996) *J. Chem. Phys.*, **105**, 3387–3397.

Gullion, T., Baker, D.B. and Conradi, M.S. (1990) *J. Magn. Reson.*, **89**, 479–484.

Hing, A.W., Vega, S. and Schaefer, J. (1992) *J. Magn. Reson.*, **96**, 205–209.

Igumenova, T.I. (2003) *Assignment of Uniformly 13C Enriched Proteins and Optimization of Their Lineshapes*, Ph.D. Thesis, Columbia, New York.

Ishii, Y., Ashida, J. and Terao, T. (1995) *Chem. Phys. Lett.*, **246**, 439–445.

Kimura, H., Nakamura, K., Eguchi, A., Sugisawa, H., Deguchi, K., Ebisawa, K., Suzuki, E. and Shoji, A. (1998) *J. Mol. Struct.*, **447**, 247–255.

Lesage, A. and Emsley, L. (2001) *J. Magn. Reson.*, **148**, 449–454.

Markley, J.L., Bax, A., Arata, Y., Hilbers, C.W., Kaptein, R., Sykes, B.D., Wright, P.E. and Wuthrich, K. (1998) *Pure Appl. Chem.*, **70**, 117–142.

Martin, R.W., Paulson, E.K. and Zilm, K.W. (2003) *Rev. Sci. Instrum.*, **74**, 3045–3061.

Martin, R.W. and Zilm, K.W. (2003) *J. Magn. Reson.*, **165**, 162–174.

Martin, R.W. and Zilm, K.W. (2004) *J. Magn. Reson.*, **168**, 202–209.

McDermott, A.E., Creuzet, F.J., Kolbert, A.C. and Griffin, R.G. (1992) *J. Magn. Reson.*, **98**, 408–413.

Morcombe, C.R. (2004) *Solid State Nuclear Magnetic Resonance of Deuterated Ubiquitin*, Ph.D. Thesis, Yale University.

Morcombe, C.R. and Zilm, K.W. (2003) *J. Magn. Reson.*, **162**, 479–486.

Neal, S., Nip, A.M., Zhang, H.Y. and Wishart, D.S. (2003) *J. Biomol. NMR*, **26**, 215–240.
Olejniczak, E.T., Vega, S. and Griffin, R.G. (1984) *J. Chem. Phys.*, **81**, 4804–4817.
Paulson, E.K., Morcombe, C.R., Gaponenko, V., Dancheck, B., Byrd, R.A. and Zilm, K.W. (2003) *J. Am. Chem. Soc.*, **125**, 15831–15836.
Reif, B., Jaroniec, C.P., Rienstra, C.M., Hohwy, M. and Griffin, R.G. (2001) *J. Magn. Reson.*, **151**, 320–327.
Reif, B., vanRossum, B.J., Castellani, F., Rehbein, K., Diehl, A. and Oschkinat, H. (2003) *J. Am. Chem. Soc.*, **125**, 1488–1489.
Rhim, W.K., Elleman, D.D., Schreibe, Lb. and Vaughan, R.W. (1974) *J. Chem. Phys.*, **60**, 4595–4604.
Rhim, W.K., Elleman, D.D. and Vaughan, R.W. (1972) *Bull. Am. Phys. Soc.*, **17**, 1182–1182.
Rhim, W.K., Elleman, D.D. and Vaughan, R.W. (1973) *J. Chem. Phys.*, **59**, 3740–3749.
Roberts, J.E., Vega, S. and Griffin, R.G. (1984) *J. Am. Chem. Soc.*, **106**, 2506–2512.
Ryan, L.M., Taylor, R.E., Paff, A.J. and Gerstein, B.C. (1980) *J. Chem. Phys.*, **72**, 508–515.
Schnell, I., Langer, B., Sontjens, S.H.M. van Genderen, M.H.P., Sijbesma, R.P. and Spiess, H.W. (2001) *J. Magn. Reson.*, **150**, 57–70.
vanRossum, B.J., Castellani, F., Pauli, J., Rehbein, K. Hollander, J. de Groot, H.J.M. and Oschkinat, H. (2003) *J. Biomol. NMR*, **25**, 217–223.
vanRossum, B.J., Forster, H. and Groot, H.J.M.de (1997) *J. Magn. Reson.*, **124**, 516–519.
Vega, A.J. (2004) *J. Magn. Reson.*, **170**, 22–41.
Vinogradov, E., Madhu, P.K. and Vega, S. (1999) *Chem. Phys. Lett.*, **314**, 443–450.
Vinogradov, E., Madhu, P.K. and Vega, S. (2001) *J. Chem. Phys.*, **115**, 8983–9000.
Waugh, J.S., Huber, L.M. and Haeberle, U. (1968) *Phys. Rev. Lett.*, **20**, 180–182.